Analysis of Super Imaging Properties of Spherical Geodesic Waveguide Using COMSOL Multyphisics

D. Grabovičkić [*], J. C. González, J. C. Miñano, P. Benítez
CEDINT, Universidad Politecnica de Madrid, Campus de Montegancedo 28223 Pozuelo, Madrid, Spain
*dejan@cedint.upm.es

Abstract: Negative Refractive Lens (NRL) has shown that an optical system can produce images with details below the classic Abbe diffraction limit using materials of negative dielectric and magnetic constants. Recently, two devices with positive refraction, the Maxwell Fish Eye lens (MFE) (Leonhardt et al 2000) and the Spherical Geodesic Waveguide (SGW)(Minano et all 2011) have been claimed to break the diffraction limit using positive refraction with a different meaning. In these cases, it has been considered the power transmission from a point source to a point receptor, which falls drastically when the receptor is displaced from the focus by a distance much smaller than the wavelength. Moreover, recent analysis of the SGW with defined object and image surfaces, which are both conical sections of the sphere, has shown that the system transmits images bellow diffraction limit. The key assumption is the use of a perfectly absorbing receptor called perfect drain. This receptor is capable to absorb all the radiation without reflection or scattering. Here, it is presented the COMSOL analysis of the SGW using a perfect drain that absorbs perfectly two modes. The design procedure for PD capable to absorb k modes is proposed, as well.

Keywords: Super-resolution, Maxwell fish-eye, Geodesic lens

1. Introduction

"Super imaging" stands for the capacity of an optical system to produce images below the wavelength of light. This can be achieved using materials with negative dielectric and magnetic constants [1][2][3][4].

Recently, a new possibility for Super-imaging has been proposed using a material with a positive, isotropic and gradient refractive index: the Maxwell Fish Eye (MFE) lens. It is well known that, in the Geometrical Optics framework, the MFE perfectly focuses rays emitted by an arbitrary point of space onto another (its image point). Leonhardt [5] demonstrated that the MFE lens in two dimensions (2D) perfectly focuses radiation of any frequency between the source and its image for 2D Helmholtz fields (which describes TE-polarized modes in a cylindrical MFE, i.e., in which electric field vector points orthogonal to the cross section of the cylinder).

This "perfect focusing" stands for the capacity of an optical system to perfectly transport an outward (monopole) 2D Helmholtz wave field, generated by a point source, towards an "infinitely-well localized drain" (which we will call "perfect point drain") located at the corresponding image point. That perfect point drain must be able to absorb totally all incident radiation, with no reflection or scattering, and the field around the drain asymptotically coincides with an inward (monopole) wave. Perfect focusing occurs in the MFE using perfect drains for an arbitrary frequency if they are located at the image point of the source [5].

Recently, it has been presented a new device, Spherical Geodesic Waveguide (SGW) for microwave frequencies [6]. The SGW is a spherical waveguide filled with a non-magnetic material and isotropic refractive index distribution proportional to $1/r$ ($\varepsilon = (r_0/r)^2$ and $\mu = 1$), r being the distance to the center of the spheres. The source and drain have been realized using the coaxial ports. Transformation Optics theory [7] proves that the TE-polarized electric modes of the cylindrical MFE are transformed into radial-polarized modes in the SGW, so both have the same imaging properties. The results presented in [8] show that this device shows up to $\lambda/500$ resolution for a discrete number of frequencies, called notch frequencies, that are close to the well known Schumman Resonance frequencies of spherical systems. For other frequencies the system does not present resolution below the diffraction limit.

The theoretical result presented by Leonhard [5], and the analysis of the SGW [8] show a concept of perfect imaging different from the NRL one presented by Pendry in [1]. In the NRL lens, the input electric field is defined on a surface. For example, a radiation emitted by the object plane (e.g. the plane xy, $z=z_0$) with tangent electric field $\mathbf{E}(x,y,z_0)$ is formed by a complete set of plane waves travelling in z direction. The optical system transmits the plane waves to the image surface (the plane xy, $z=z_1$) generating the same field $\mathbf{E}(x,y,z_0)= \mathbf{E}(x,y,z_1)$. In particular, if the field in the object plane is $\mathbf{E}(x,y,z_0)=\delta(x,y)\mathbf{y}$ (Dirac delta), the field in the image plane is $\mathbf{E}(x,y,z_1)=\delta(x,y)\mathbf{y}$,

In the theoretical results for the MFE and SGW, the concept of object and image surface does not exist, since the source and drain are points. However, recently, the concept of object and image surface has been implemented in the SGW as well (similarly as done by Pendry) [9]. The object surface is $\theta=\theta_0$ (equivalent to $z=z_0$ of the NRL) and the image surface is $\theta_1=\pi-\theta_0$ (equivalent to $z=z_1$ of the NRL, Figure 1. The analysis is done for TE modes depending only on the spherical coordinates (θ,φ), that is, the electric field has the expression $\mathbf{E}(r,\theta,\varphi)=E(\theta,\varphi)\mathbf{r}$.
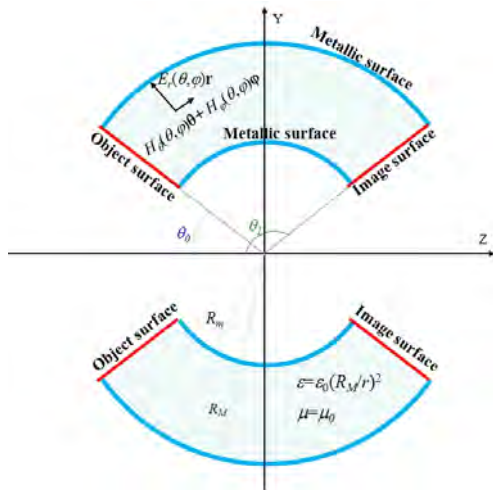
Figure 1 Spherical Geodesic Waveguide. Definition of the object and image surface

In [9], it has been shown that if the field $\mathbf{E}(\theta_0,\varphi)$ in the object surface has spatial distribution with thickness much smaller than the wavelength (e.g. less than $\lambda/100$), then the field in the image surface has also spatial distribution with thickness much smaller than the wavelength. For example, a Dirac delta field $E(\theta_0,\varphi)\mathbf{r}= \delta(\varphi-3\pi/2)\mathbf{r}$ in the object

surface is represented as a sum of the first 2000 terms of the Fourier Series, thus the thickness of the field is around $\lambda/450$ ([9]). The same shape of the field is obtained in the image surface, as well. These results show that a point source on the object surface can be focused on a point of the image surface without wavelength limitation.

A necessary condition for the perfect imaging in [9] is existence of a perfect drain in the image surface. This drain absorbs perfectly all the modes transmitted in the SGW. However, in [9] it has been introduced only as a theoretical concept.

Here we analyze the SGW system having a compound structure in the object surface acting as a perfect drain. This perfect drain consists of two conical solids made of materials with complex permittivities (see Figure 3). Using these two materials we are able to perfectly absorb two modes. Unfortunately, we are not able to absorb more than two modes (e.g. in [9] the theoretical perfect drain absorbed 2000 modes), so we can not perfectly image the Dirac delta electric field (since we would have to absorb perfectly all the modes). Herein, the electric field will be represented by a sum of two cosines (two modes). This field will be perfectly absorbed in the image surface.

2. SGW with perfect drain

The SGW is formed by two concentric metallic spheres. The object surface is $\theta=\theta_0$ and the image surface is $\theta=\pi-\theta_0$. Due to the symmetry of the problem, the electric field has only r component and does not depend on the coordinate r. The magnetic field has components θ, φ and does not depend on the coordinate r:

$$\mathbf{E}(r,\theta,\varphi) = E_r(\theta,\varphi)\mathbf{r}$$
$$\mathbf{H}(r,\theta,\varphi) = H_\theta(\theta,\varphi)\boldsymbol{\theta} + H_\varphi(\theta,\varphi)\boldsymbol{\varphi} \quad (1)$$

The relative dielectric and magnetic constants inside the SGW are given as

$$\varepsilon(r,\theta,\varphi) = \varepsilon_0 \left(\frac{R_M}{r} \right)^2 \quad \mu(r,\theta,\varphi) = \mu_0 \quad (2)$$

The electric and magnetic fields $\mathbf{E}$ and $\mathbf{H}$ satisfy the next equation:

$$\mathbf{E}(\theta,\varphi) = E(\theta)e^{jn\varphi}\mathbf{r}$$
$$\mathbf{H}(\theta,\varphi) = \frac{\nabla \times \mathbf{E}(\theta,\varphi)}{-j\omega\mu_0} =$$
$$= e^{jn\varphi}\left[-\frac{E(\theta)jn}{\sin(\theta)}\boldsymbol{\theta} + \frac{dE(\theta)}{d\theta}\boldsymbol{\varphi} \right]\frac{1}{j\omega\mu_0 r} \quad (3)$$

From the second Maxwell equation:

$$\mathbf{E}(\theta,\varphi) = \frac{\nabla \times \mathbf{H}(\theta,\varphi)}{j\omega\varepsilon}$$

$$\frac{d}{d\theta}\left(\sin(\theta)\frac{dE(\theta)}{d\theta}\right) + \tag{4}$$

$$E(\theta)\left((k_0 R_M)^2 \sin(\theta) - \frac{n^2}{\sin(\theta)}\right) = 0$$

The solution of Eq. (4) is:

$$E(\theta) = AP_\nu^n(\cos(\theta)) + BQ_\nu^n(\cos(\theta)) \tag{5}$$

$$\upsilon(\upsilon+1) = (k_0 R_M)^2$$

where $P_\nu^n(x)$ and $Q_\nu^n(x)$ are the Legendre functions of first and second type, A and B integration constants and n an integer constant (since $\mathbf{E}(\theta,0) = \mathbf{E}(\theta,2\pi)$).

The electric field can be expressed as follows:

$$E(\theta) = E_f F_\nu^n(\cos(\theta)) + E_r R_\nu^n(\cos(\theta))$$

$$F_\nu^n(\cos(\theta)) = P_\nu^n(\cos(\theta)) + ja\frac{2}{\pi}Q_\nu^n(\cos(\theta)) \tag{6}$$

$$R_\nu^n(\cos(\theta)) = P_\nu^n(\cos(\theta)) - ja\frac{2}{\pi}Q_\nu^n(\cos(\theta))$$

where $F_\nu^n(x)$ and $R_\nu^n(x)$ are called forward and reverse waves, E_f, E_r are constants and $a=1$.

In accordance with the Uniqueness Theorem [10] if the tangential electric field is known in the boundary surface of a finite volume, the fields are completely determined inside the volume. In the metallic surfaces the tangential electric field is null, while in the surfaces $\theta=\theta_0$ and $\theta=\pi-\theta_0$ it can be developed using Fourier series:

$$\mathbf{E}(\theta_0,\varphi) = \sum_n A_n e^{jn\varphi}\mathbf{r}$$

$$\mathbf{E}(\pi-\theta_0,\varphi) = \sum_n B_n e^{jn\varphi}\mathbf{r} \tag{7}$$

The fields $\mathbf{E}$ and $\mathbf{H}$ are developed in modes (see Eq. (4), (5) and (6))

$$\mathbf{E}(\theta,\varphi) = \sum_n \left[E_{fn}F_\nu^n(l) + E_{rn}R_\nu^n(l)\right]e^{jn\varphi}\mathbf{r}$$

$$\mathbf{H}(\theta,\varphi) = \frac{1}{j\omega\mu_0}\sum_n e^{jn\varphi}\left[\begin{array}{l}\dfrac{-(E_{fn}F_\nu^n(l) + E_{rn}R_\nu^n(l))jn}{\sin(\theta)}\boldsymbol{\theta} + \\ \dfrac{d(E_{fn}F_\nu^n(l) + E_{rn}R_\nu^n(l))}{d\theta}\boldsymbol{\varphi}\end{array}\right]$$

$$\tag{8}$$

where $l=\cos(\theta)$.

The coefficients E_{fn} and E_{rn} can be obtained from the boundary conditions:

$$E_{fn}F_\nu^n(\cos(\theta_0)) + E_{rn}R_\nu^n(\cos(\theta_0)) = A_n$$

$$E_{fn}F_\nu^n(\cos(\pi-\theta_0)) + E_{rn}R_\nu^n(\cos(\pi-\theta_0)) = B_n \tag{9}$$

In [9] it has been considered a Dirac delta field in the object surface. This function has been represented as a sum of the first 2000 terms of the Fourier Series. Using a theoretical perfect drain, all the modes were absorbed perfectly in the image surface, making a perfect image of the input field.

Consider now an input electric field containing only one mode

$$\mathbf{E}(\theta_0,\varphi) = e^{jn_1\varphi} \tag{10}$$

where n_1 is an integer. Let calculate a drain which absorbs this field. We are going to put only one material that occupies the entire conical hole (from $\theta=\pi-\theta_0$ to $\theta=\pi$), Figure 2. We have to put two conditions: there is no any reflected wave in the guide and at $\theta=\pi$ the electric field is finite. Assume the form of the electric field in the drain as

$$S_\nu^{n_1}(\cos(\theta)) = P_\nu^{n_1}(\cos(\theta)) + AQ_\nu^{n_1}(\cos(\theta)) \tag{11}$$

Let find now a proper linear combination of the Legendre functions for the electric field inside the drain to fulfill the two established conditions. According to Eq. (11) and the properties of the Legendre functions [12], this can be achieved if $A=-2\tan(\pi\nu)/\pi$ in Eq. (11).
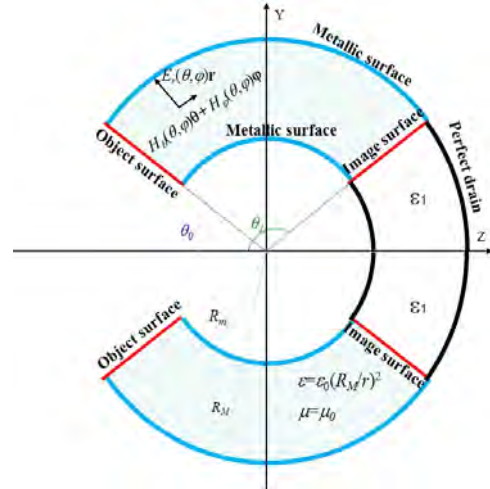
Figure 2 Spherical Geodesic Waveguide with one-layer perfect drain

If there is no any reflection at the boundary $\theta_1=\pi-\theta_0$, the electric field inside the SGW contains only forward wave $F_{\nu_0}^{n_1}$. In order to calculate the permittivity of the perfect drain, we have to establish the following conditions: The equality of the electric field at $\theta_1=\pi-\theta_0$

$$E_0 F_{\nu_0}^{n_1}(\cos(\theta_1)) = E_1 S_{\nu_1}^{n_1}(\cos(\theta_1)) \tag{12}$$

where ν_0 is calculated using Eq.(5). This variable depends on the material inside the SGW and the work frequency.

The equality of the tangential field **B** (**B**=μ**H**) at θ_1.

$$E_0 \frac{dF_{v_0}^0 (\cos(\theta_1))}{d\theta} = E_1 \frac{dS_{v_1}^0 (\cos(\theta_1))}{d\theta} \qquad (13)$$

The equality of the normal field **H** at $\theta=\pi-\theta_0$.

$$\frac{E_0 F_{v_0}^0 (\cos(\theta_1))}{j\omega\mu_0 \sin(\theta_1)} = \frac{E_1 S_{v_1}^0 (\cos(\theta_1))}{j\omega\mu_0 \sin(\theta_1)} \qquad (14)$$

Equations (12) and (14) are identical, hence dividing Eq. (12) and Eq.(13) we get the next equation

$$\frac{F_{v_0}^0 (\cos(\theta_1))}{\dfrac{dF_{v_0}^0 (\cos(\theta_1))}{d\theta}} = \frac{S_{v_1}^0 (\cos(\theta_1))}{\dfrac{dS_{v_1}^0 (\cos(\theta_1))}{d\theta}} \qquad (15)$$

where v_1 is the unknown variable. Then, the permittivity of the perfect drain ε_{PD} is obtained using the next equation

$$v_1(v_1 +1) = \left(\frac{2\pi f}{c} R_M\right)^2 \varepsilon_{PD} \qquad (16)$$

This result has already been presented for the equivalent MFE lens in [11].
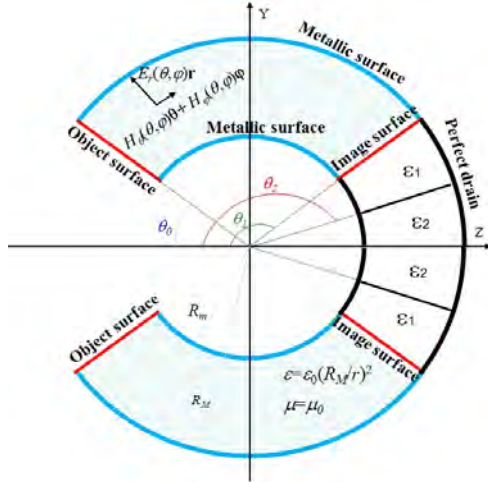
Figure 3 Spherical Geodesic Waveguide with two-layer perfect drain

Consider now the case when we have two modes to absorb. Therefore, we have to put two dissipative regions: one having v_1 for $\theta_2 > \theta > \theta_1$, and another one having v_2 for $\pi > \theta > \theta_2$ (see Figure 3). In the SGW we have only incident wave (since the drain absorbs perfectly), in the first region of the drain (defined by v_1) there are an incident and a reflected wave, and finally, in the second region of the drain there is only a wave represented by function $S_v^n(\cos(\theta))$. Imposing the equality of the electric and magnetic fields at the borders θ_1 and θ_2 for the two modes we have a system of equations

$$l_1 = \cos(\theta_1), \quad l_2 = \cos(\theta_2)$$

$$E_{0n} F_{v_0}^n (l_1) = E_{1in} F_{v_1}^n (l_1) + E_{1rn} R_{v_1}^n (l_1)$$

$$E_{1in} F_{v_1}^n (l_2) + E_{1rn} R_{v_1}^n (l_2) = E_{2n} S_{v_2}^n (l_2) \qquad (17)$$

$$E_{0n} \frac{dF_{v_0}^n (l_1)}{d\theta} = E_{1in} \frac{dF_{v_1}^n (l_1)}{d\theta} + E_{1rn} \frac{dR_{v_1}^n (l_1)}{d\theta}$$

$$E_{1i0} \frac{dF_{v_1}^0 (l_2)}{d\theta} + E_{1r0} \frac{dR_{v_1}^0 (l_2)}{d\theta} = E_{20} \frac{dS_{v_2}^0 (l_2)}{d\theta}$$

where n is mode number. We have to apply this system twice for two modes n_1 and n_2 to obtain 8 equations. E_{0in1} and E_{0i0n2} are constants since they are represented the incident wave in the SGW guide, also v_0 is a known value, while E_{1in1}, E_{1rn1}, E_{2n1}, E_{1n21}, E_{1rn2}, E_{2n2}, v_1 y v_2 are 8 unknown functions. After solving the system, we get the values for the permittivities ε_1 and ε_2.

In general this procedure can be extended to k modes, k being a number higher than 2. In order to absorb k modes, the perfect drain has to be realized with k layers having different permittivities. However the system is not linear, and even for k=2, we have solved it using an iteration method. Unfortunately, up to now we did not solve it for higher k.

3. Simulations in COMSOL Multiphysics

The simulation has been done using 3D RF Modul in COMSOL Multiphysics. The SGW has been modeled with the following geometrical parameters:

$$\theta_0 = \frac{\pi}{5}, \theta_1 = \frac{4\pi}{5}, \theta_2 = \frac{9\pi}{10}, \lambda = 0.931138 \text{ m} \qquad (18)$$
$$v_0 = 6.3, R_M = 1.005 \text{ m}, R_m = 1 \text{ m}$$

The refractive index between the metallic spherical shells is $n(r)=R_m/r$. The shells are considered as perfect conductors.

Special care has be taken to define the mesh of the system. In order to mesh the guide properly, the geometry has been divided into few domains. Each domain is meshed separately according to its geometric and physical properties. Since the guide thickness is very low $(R_M-R_m)/R_m \ll 1$, the SGW is meshed using a swept mesh (2D triangular mesh from the outer surface is swept to the inner surface, as presented in Figure 4). The mesh density increases close to the object and image surfaces in order to obtain higher resolution of the results.

The electric field in the object surface containing two modes $n=1$ and $n=2$ (the first and the second one) is given by the next term

$$\mathbf{E}(\theta_0, \varphi) = e^{j\varphi} + e^{j2\varphi} \qquad (19)$$

This input electric field is defined in the COMSOL simulation using the Electric field boundary conditions. The permittivities of each perfect drain layer have been calculated using the procedure presented in the previous section. These are the results

$$\varepsilon_1 = 1.07003 - i \cdot 0.398973$$
$$\varepsilon_2 = 1.84269 - i \cdot 1.66792 \qquad (20)$$
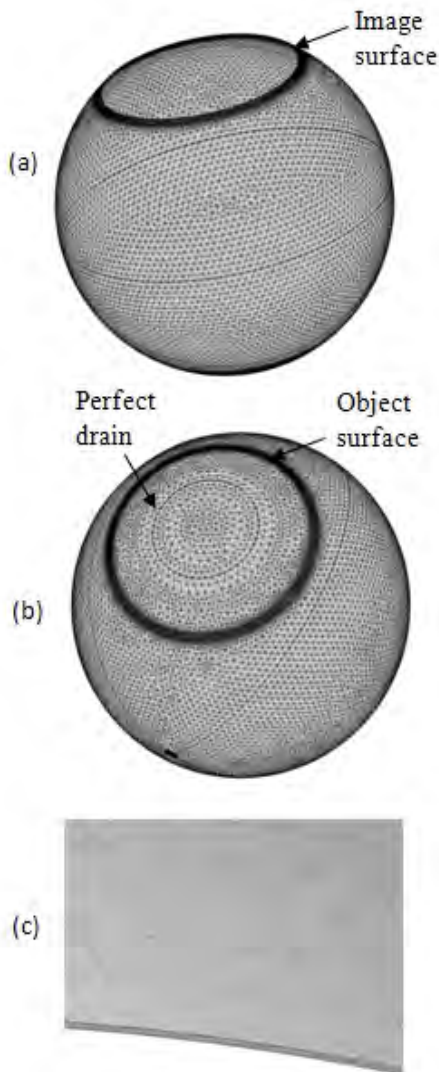
Figure 4 Mesh structure. (a) Object side of the SGW , (b) Image side of the SGW (c) close up of the SGW wall showing the mesh distribution

Figure 5 and Figure 6 show the graphs of the electric and magnetic field in the object and image surface obtained in the COMSOL simulation. The electric field has only the radial component. The magnetic field has H_θ

and H_φ components. We have presented only H_φ components of the magnetic field since the shape of the H_θ component is the same as the radial component of the electric field. In all the graphs, the horizontal axis denotes the φ coordinate (from $-\pi$ to π).
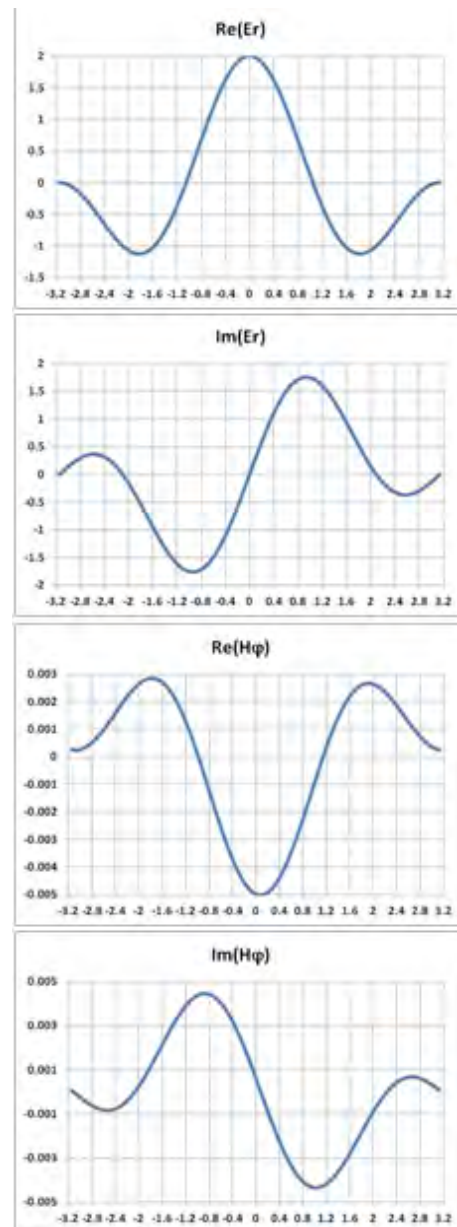
Figure 5 Real and imaginary parts of the radial electric field and tangential magnetic field in the object surface

Consider now the theoretical results. If there were not any reflection in the image surface, the electric field inside the SGW should have only forward component. According to Eq.(9), if there is only forward component, we get the following results
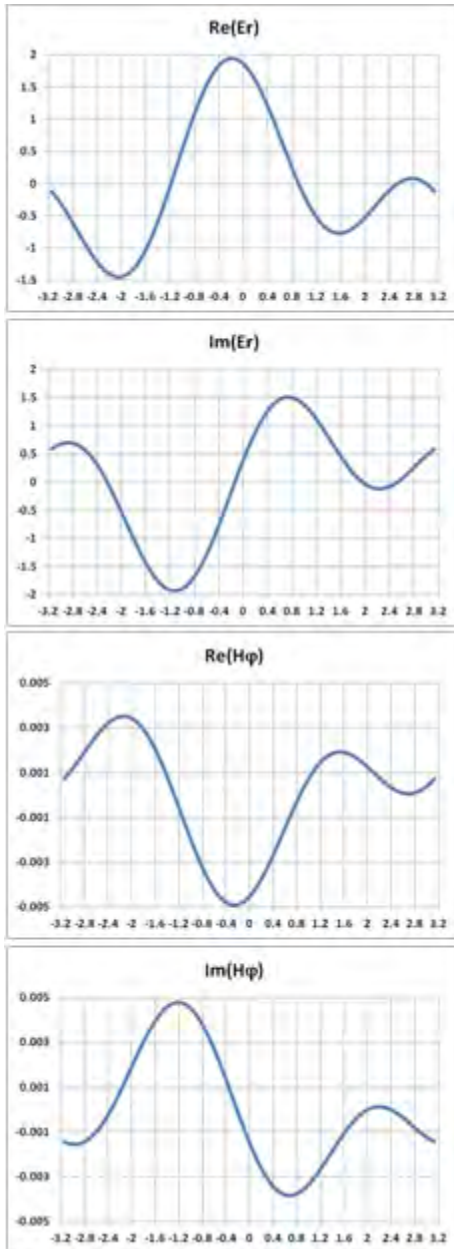
Figure 6 Real and imaginary parts of the radial electric field and tangential magnetic field in the image surface

$$E_{f1} = \frac{1}{F^1_{v_0}(\cos(\theta_0))} F^1_{v_0}, \quad E_{r1} = 0$$

$$E_{f2} = \frac{1}{F^2_{v_0}(\cos(\theta_0))} F^2_{v_0}, \quad E_{r2} = 0$$

(21)

The electric and magnetic fields in the image surface $\mathbf{E}(\theta_l,\varphi)$, $\mathbf{H}(\theta_l,\varphi)$, are then obtained using Eq.(8). We have compared these theoretical results and the results obtained in the COMSOL simulation and we concluded that they are the same. This means that Figure 5 and Figure 6 represent both results, obtained theoretically and in the COMSOL simulation.

Since the results calculated in COMSOL are the same as the theoretical ones, which are obtained under assumption of perfect absorption, we can conclude that there is no any reflection in the image surface.

Unfortunately we could not resolve the system for more modes, thus we could not set the COMSOL simulation for the case when the input electric field is a Dirac delta function.

4. Conclusions

In the previous works, it has been demonstrated that the Spherical Geodesic Waveguide (SGW) show super-resolution up to $\lambda/500$ for a point source. Also, recently it is shown that a Dirac delta electric field defined in a conical section of the SGW is transmitted to the same Dirac delta electric field at another conical section on the other side of the guide. This has been achieved using a theoretical concept of perfect drain which was capable to absorb all the incident modes in the guide. This theoretical drain can be realized using a drain containing a multi-layer structure having different permittivities in each layer. Here we have presented the procedure for calculating this multi-layer drain capable to absorb k modes. However, up to now, we have solved it only for $k=2$. The theoretical results coincide with the COMSOL simulation.

5. References

1. J. B. Pendry, Negative Refraction makes a Perfect Lens, *Phy. Review Let.*, **85,** 3966-3989 (2000)
2. R. A. Shelby et al, Experimental verification of negative index of refraction, *Science*, **292**, 79 (2001)
3. N Fang et al, Sub-Diffraction-Limited Optical Imaging with a Silver Superlens, *Science*, **308**, 534-537 (2005)
4. F Mesa et al, Three dimensional superresolution in material slab lenses: Experiment and theory, *Phy. Review B*, **72**, 235117 (2005)
5. U. Leonhardt, Perfect imaging without negative refraction, *New J. Phys.*, **11**, 093040 (2009)
6. J.C Miñano et al, Perfect imaging with geodesic waveguides. *New Journal of Physics*, **12**, 123023 (2010)
7. U.Leonhardt, *Geometry and Light: The Science of Invisibility*, Dover (2010)
8. J.C Miñano et al, Super-resolution for a point source better than λ/500 using positive

refraction, *New Journal of Physics*, **13**, 125009 (2011)

9. J.C González et al, Negative refractive perfect lens vs Spherical geodesic lens. Perfect Imaging comparative analysis, *ArXiv*, 1204.2672v1 (2012).

10. J.A Stratton, *Electromagnetic Theory*, McGraw-Hill (1941)

11. J.C González et al, Perfect drain for the Maxwell Fish Eye lens, *New Journal of Physics*, **13,** 023038 (2011)

12. A. Erdélyi et al, *Higher Transcendental Functions vol I* , New York: McGraw-Hill (1953)

6. Acknowledgments